British Journal of Pharmacology

DOI:10.1111/bph.13238
www.brjpharmacol.org

RESEARCH PAPER

The novel PAR2 ligand C391 blocks multiple PAR2 signalling pathways *in vitro* and *in vivo*

Scott Boitano[1,2], Justin Hoffman[1,2], Andrea N Flynn[1,2], Marina N Asiedu[3], Dipti V Tillu[3], Zhenyu Zhang[2], Cara L Sherwood[1,2], Candy M Rivas[1,2,4], Kathryn A DeFea[5], Josef Vagner[2] and Theodore J Price[2,3,6]

[1]*Arizona Respiratory Center and Department of Physiology,* [2]*The BIO5 Collaborative Research Institute,* [3]*Department of Pharmacology,* [4]*Graduate Interdisciplinary Program in Physiological Sciences, University of Arizona, Tucson, AZ, USA,* [5]*Biomedical Sciences Division, University of California, Riverside, CA, USA, and* [6]*School of Behavioral and Brain Sciences, University of Texas at Dallas, Dallas, TX, USA*

Correspondence
Scott Boitano, Arizona Respiratory Center, University of Arizona, 1501 N. Campbell Avenue, Tucson, AZ 85724-5030, USA; E-mail: sboitano@email.arizona.edu; Theodore J. Price, School of Behavioral and Brain Sciences, University of Texas at Dallas, JO 4.212, 800 W. Campbell Road, Richardson, TX 75080, USA. E-mail: Theodore.price@utdallas.edu

Received
28 January 2015
Revised
18 June 2015
Accepted
28 June 2015

BACKGROUND AND PURPOSE

Proteinase-activated receptor-2 (PAR2) is a GPCR linked to diverse pathologies, including acute and chronic pain. PAR2 is one of the four PARs that are activated by proteolytic cleavage of the extracellular amino terminus, resulting in an exposed, tethered peptide agonist. Several peptide and peptidomimetic agonists, with high potency and efficacy, have been developed to probe the functions of PAR2, *in vitro* and *in vivo*. However, few similarly potent and effective antagonists have been described.

EXPERIMENTAL APPROACH

We modified the peptidomimetic PAR2 agonist, 2-furoyl-LIGRLO-NH_2, to create a novel PAR2 peptidomimetic ligand, C391. C391 was evaluated for PAR2 agonist/antagonist activity to PAR2 across G_q signalling pathways using the naturally expressing PAR2 cell line 16HBE14o-. For antagonist studies, a highly potent and specific peptidomimetic agonist (2-aminothiazo-4-yl-LIGRL-NH_2) and proteinase agonist (trypsin) were used to activate PAR2. C391 was also evaluated *in vivo* for reduction of thermal hyperalgesia, mediated by mast cell degranulation, in mice.

KEY RESULTS

C391 is a potent and specific peptidomimetic antagonist, blocking multiple signalling pathways (G_q-dependent Ca^{2+}, MAPK) induced following peptidomimetic or proteinase activation of human PAR2. In a PAR2-dependent behavioural assay in mice, C391 dose-dependently (75 μg maximum effect) blocked the thermal hyperalgesia, mediated by mast cell degranulation.

CONCLUSIONS AND IMPLICATIONS

C391 is the first low MW antagonist to block both PAR2 Ca^{2+} and MAPK signalling pathways activated by peptidomimetics and/or proteinase activation. C391 represents a new molecular structure for PAR2 antagonism and can serve as a basis for further development for this important therapeutic target.

Abbreviations

16HBE14o-, immortalized human bronchial epithelial cell line; 2-f-LIGRLO-NH_2, 2-furoyl-Leu-Ile-Gly-Arg-Leu-Orn(Aloc)-NH_2; 2-at-LIGRL-NH_2, 2-aminothiazo-4-yl-Leu-Ile-Gly-Arg-Leu-NH_2; $[Ca^{2+}]_i$, intracellular free calcium ion concentration; C391, (2*S*)-6-amino-N-((*S*)-1-(((*S*)-1-amino-3-(4-hydroxyphenyl)-1-oxopropan-2-yl)amino)-4-methyl-1-oxopentan-2-yl)-2-((3*S*)-1-(furan-2-carbonyl)-3-(3-methylbutanamido)-4,7-dioxooctahydro-8*H*-pyrazino[1,2-a]pyrimidin-8-yl)hexanamide; GB88, 5-isoxazoyl-Cha-Ile-spiroindene-1,4,-piperidine; HBSS, Hank's balanced salt solution; HR-MS, high-resolution mass spectroscopy; ICW, in-cell Western blotting; K-14585, N-[1-(2,6-dichlorophenyl)methyl]-3-(1-pyrrolidinylmethyl)-1H-indol-5-yl]aminocarbonyl}-glycinyl-L-lysinyl-L-phenylalanyl-N-benzhydrylamide; MCS, matrix coating solution; RTCA, xCELLigence real time cell analyser

Tables of Links

TARGETS
GPCRs[a]
PAR2
Enzymes[b]
ERK1/2
p38 MAP kinase

LIGANDS
2-f-LIGRLO-NH_2
GB88

These Tables list key protein targets and ligands in this article which are hyperlinked to corresponding entries in http://www.guidetopharmacology.org, the common portal for data from the IUPHAR/BPS Guide to PHARMACOLOGY (Pawson *et al.*, 2014) and are permanently archived in the Concise Guide to PHARMACOLOGY 2013/14 ([a,b]Alexander *et al.*, 2013a,b).

Introduction

The proteinase-activated receptor-2 (PAR2) is one of the four members of the family of GPCRs that are activated after proteolytic cleavage of their extracellular, amino terminus (Adams *et al.*, 2011; Ramachandran *et al.*, 2012). The resulting 'tethered-peptide' sequence (ending with SLIGRL in the rodent receptor and SLIGKV in the human receptor) exposed after proteolytic cleavage activates PAR2. A variety of potent and effective peptidomimetic agonists based upon the exposed tethered sequences have been developed to PAR2 (Adams *et al.*, 2011; Boitano *et al.*, 2014). These compounds have been very useful in understanding the consequences of PAR2 activation across experimental models. However, the natural tethered agonist presentation for PAR2, and its corresponding access to the PAR2 binding pocket, has proved a difficult target for development of antagonists. Despite this difficulty, a number of PAR2 antagonists have been proposed (Suen *et al.*, 2012; Yau *et al.*, 2013). Further complicating the issue of drug development is the growing evidence for 'biased signalling' that can follow PAR2 agonism (Hollenberg *et al.*, 2014) or antagonism (Goh *et al.*, 2009; Suen *et al.*, 2014).

PAR2 plays an important role in a variety of diseases linked to proteinase release from endogenous sources or exposure to exogenous proteinases (Ramachandran *et al.*, 2012; Hollenberg *et al.*, 2014). One consequence of PAR2 activation in the peripheral nervous system is sensitization of neurons responsible for transmitting noxious information to the CNS. These nociceptive neurons express PAR2, and PAR2 activation on these neurons leads to enhanced signalling via a variety of channels including the capsaicin and noxious heat receptor, TRPV1 (Dai *et al.*, 2004). PAR2 is responsible for proteinase sensitization of TRPV1 *in vivo*, leading to thermal hyperalgesia. PAR2 null animals have deficits in pain sensitization in a variety of inflammatory pain models, and PAR2 activation is sufficient to induce a transition to a chronic pain state, making this receptor an important target for drug development for pathological pain (Vergnolle, 2009; Bao *et al.*, 2014; Tillu *et al.*, 2015). Additionally, a broad variety of pre-clinical and clinical findings link exogenous proteinases, and more specifically PAR2, to asthma (Reed and Kita, 2004; Vergnolle, 2009; Jacquet, 2011; Snelgrove *et al.*, 2014). While there is a strong rationale for PAR2 antagonist drug discovery for these indications, few PAR2 antagonists have been described and even fewer have been demonstrated to exhibit efficacy in pre-clinical disease models (Yau *et al.*, 2013).

Here, we describe a novel PAR2 antagonist based upon structures from previously described peptidomimetic PAR2 agonists. This compound, C391 [(2*S*)-6-amino-N-((*S*)-1-(((*S*)-1-amino-3-(4-hydroxyphenyl)-1-oxopropan-2-yl)amino)-4-methyl-1-oxopentan-2-yl)-2-((3*S*)-1-(furan-2-carbonyl)-3-(3-methylbutanamido)-4,7-dioxooctahydro-8*H*-pyrazino[1,2-a]pyrimidin-8-yl)hexanamide], attenuates PAR_2 signalling via Ca^{2+} and MAPK pathways and is efficacious *in vivo*. C391 is structurally distinct from all previously described PAR2 antagonists and therefore represents a new lead for further PAR2 antagonist discovery.

Methods

Compound syntheses

Compound C391 (Figure 1) was synthesized by solid phase methodology using Fmoc strategy on a base labile Sheppard's hydroxymethyl-benzoic acid linker (Atherton *et al.*, 1981). The azabicycloalkane scaffold was cyclized on the resin by

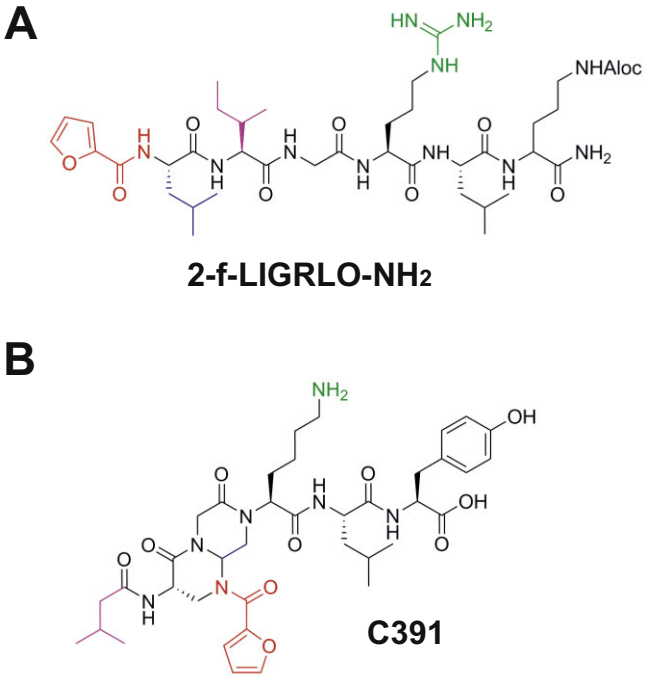

Figure 1

Structural comparison of PAR2 ligands 2-furoyl-LIGRLO-NH_2 and C391. The chemical structures for (A) the known PAR2 agonist 2-furoyl-LIGRLO-NH_2 and (B) the novel peptidomimetic compound 391 (C391) are shown; colour coding denotes predicted surrogates between the two structures. The 2-furoyl-amide heterocycle is shown in red. The Leu residue in peptide A (blue) is mimicked by part of the azabicycloalkane scaffold in C391. The Ile residue (violet) is substituted with isobutyl side-decoration of azabicycloalkane in C391. The positively charged Arg (green) is substituted with a Lysine-like group in C391. The Leu-Tyr C-terminal dipeptide on C391 is not derived from peptide A.

diluted formic acid, followed by basic cleavage (0.1 M NaOH) of the product from the resin. The crude product was purified by preparative HPLC on a 22 × 250 mm reverse-phase column. The structure was confirmed by NMR and high-resolution mass spectroscopy (HR-MS).

PAR2 activating peptidomimetics, 2-aminothiazo-4-yl-Leu-Ile-Gly-Arg-Leu-NH_2 (2-at-LIGRL-NH_2), 2-furoyl-Leu-Ile-Gly-Arg-Leu-Orn(Aloc)-NH_2 (2-f-LIGRLO-NH_2) and compound GB88 (5-isoxazoyl-Cha-Ile-spiroindane-1,4piperidine) were synthesized as previously described (Barry *et al.*, 2010; Flynn *et al.*, 2011; Hoffman *et al.*, 2012). All compounds were purified by preparative HPLC and the structures were confirmed by HR-MS and HPLC.

Tissue culture

16HBE14o- (immortalized human bronchial epithelial cell line) cells, an SV40 transformed human bronchial epithelial cell line (Gruenert *et al.*, 1995), were obtained through the California Pacific Medical Center Research Institute (San Francisco, CA, USA). The cells were maintained and expanded as previously described (Flynn *et al.*, 2013). Cell lines were expanded in tissue culture flasks prior to transfer to glass coverslips or 96-well plates for experiments. Cultureware was coated initially with a matrix coating solution (MCS: 88% LHC basal medium, 10% BSA, 1% bovine collagen type I and 1% human fibronectin) and incubated for 2 h at 37°C, after which the coating solution was removed and allowed to dry for at least 1 h. 16HBE14o- cells were plated onto the cultureware at a concentration of 1×10^5 cells·cm^{-2} and grown in Eagle's minimal essential medium supplemented with 10% FBS, 2 mM glutamax, penicillin and streptomycin (growth medium) at 37°C in a 5% CO_2 atmosphere. Growth medium was replaced every other day until the cells reached proper cell density for experimentation.

In vitro *physiological response with real-time cell analysis*

16HBE14o- cells on E-plates in growth medium and in a 37°C, 5% CO_2 incubator were monitored for the establishment of, and changes in, impedance overnight every 15 min using the xCELLigence™ real time cell analyser (RTCA; ACEA Biosciences, San Diego, CA, USA) (Atienza *et al.*, 2005; Flynn *et al.*, 2013). When cells reached appropriate impedance the next day, and prior to the experiment, the RTCA was moved to room air and temperature where full growth medium was replaced with 100 µL of modified Hank's balanced salt solution (HBSS) pre-warmed to 37°C. The RTCA was then allowed to reach room temperature (45 min) prior to ligand addition. Each well was then supplemented with 100 µL of HBSS containing appropriate concentrations of 2-at-LIGRL-NH_2 and/or C391 ligands in quadruplicate. Additional wells were used for vehicle controls. Relative impedance in each well was monitored every 30 s over 4 h. Traces were normalized for experimental start time and baselined to ligand-free-treated cells as described (Flynn *et al.*, 2013).

Intracellular Ca^{2+} concentration ($[Ca^{2+}]_i$) signalling

$[Ca^{2+}]_i$ was measured using digital imaging microscopy as previously described (Flynn *et al.*, 2013), with slight modifications. Coverslip cultures were washed with HBSS and loaded for 45 min in 5 µM fura 2-AM in HBSS. Fura 2 fluorescence was observed on an Olympus IX70 microscope (Waltham, MA, USA) with a 40× oil immersion objective after alternating excitation between 340 and 380 nm by a 75 W Xenon lamp linked to a Delta Ram V illuminator (PTI, London, Ontario, Canada) and a gel optic line. Images were captured using an Evolve camera (Roper Scientific, Tucson, AZ, USA) under EasyRatioPro software (PTI). $[Ca^{2+}]_i$ for each individual cell in the field of view was calculated from captured images by ratiometric analysis using equations originally published in Grynkiewicz *et al.* (1985). A minimum of one ratio per second was calculated for all experiments <10 min. For 20 min experiments presented in the Supporting Information, one ratio per 3 seconds were captured over the first 15 min, and one ratio per second over the final 5 min. Line drawings representing $[Ca^{2+}]_i$ traces over time are mean $[Ca^{2+}]_i$ of all cells within a field of view (80–110) and are representative of at least four experiments. Ca^{2+} response graphs are the percentage of cells that increase $[Ca^{2+}]_i$ above 150 nM within the 3 min experimental time frame that included agonist addition. Inhibition experiments included a 2 min pre-exposure to antagonists prior to the addition of

agonist/antagonist combination, unless otherwise noted. Agonists included the PAR2-specific peptidomimetic 2-at-LIGRL-NH_2 (Flynn *et al.*, 2011) and porcine pancreas trypsin (5 nM; Sigma-Aldrich T-0303, St. Louis, MO, USA). Ca^{2+} concentration–response curves and IC_{50} values were calculated from Ca^{2+} response experiments using GraphPad Prism software (GraphPad Software Inc., San Diego, CA, USA).

Detection of MAPK signalling

In-cell Western (ICW) studies were performed as previously described (Flynn *et al.*, 2011) with modification to assess antagonistic responses. 16HBE14o- cells were grown to confluence on black-walled 96-well plates pre-coated with MCS. Cells were exposed to a range of concentrations of C391 from 300 nM to 100 μM for 2 min at room temperature. Cells were then exposed to PAR2-specific peptidomimetics (2.5 μM 2-at-LIGRL-NH_2) in the presence of C391 for an additional 5 min, fixed, incubated in primary antibody (rabbit anti-pERK; Cell Signaling Technologies, Danvers, MA, USA), secondary antibody (Invitrogen, Life Technologies, Grand Island, NY, USA), nuclear stain DRAQ5 (Cell Signaling Technologies) and imaged on an Odyssey Scanner (LI-COR, Lincoln, NE, USA) as per manufacturers' instructions. For Western blot experiments, 16HBE14o- cells were plated on MCS-coated 6-well plates. Once cells reached confluence, the culture medium was removed, cells were pre-treated with C391 for 1 min and then exposed to PAR2 agonist with C391 for an additional 5 min. Agonist/antagonist was removed, and cells were lysed in a modified radioimmune precipitation assay buffer [50 mM Tris (pH 7.4), 150 mM NaCl, 1 mM EDTA (pH 8.0), 1% Triton X-100]. Lysates were sonicated for 10 min at 4°C, centrifuged for 15 min at 14 000× *g* and stored at –80°C until blot analysis. Both activated ERK1/2 [phosphorylated ERK (pERK)] and non-activated ERK1/2 (total ERK; tERK), were assayed by standard SDS-PAGE (antibodies from Cell Signaling Technology).

Animal welfare and ethical statement

All animal care and experimental protocols were approved by the Institutional Animal Care and Use Committee of The University of Arizona. These procedure comply with the ARRIVE guidelines (Kilkenny *et al.*, 2010; McGrath *et al.*, 2010). All experimental procedures were as humane as possible. A total of 20 animals were used in the experiments described here.

In vivo *thermal hyperalgesia*

Male ICR mice (Harlan, Houston, TX, USA) weighing 25–30 g were used for these studies. Mice were placed in Plexiglas boxes for habituation and then baseline thermal latencies were assessed using the method of Hargreaves *et al.* (1988). Mice received intraplantar injections of 0.2 μg Compound 48/80 (Sigma-Aldrich) (Vergnolle *et al.*, 2001) with or without indicated concentrations of C391 in a total volume of 25 μL through a 31 gauge needle. Thermal latencies were then assessed at the indicated time points over a total of 180 min. Experimental measurements were performed by observers unaware of the treatments and animals were randomized to groups (3–8 mice) by drawing numbers.

Data analysis

All statistical analyses were performed with GraphPad Prism software (GraphPad Software Inc.). Curve fitting was carried out using non-linear regression with variable slope. Multivariate comparisons were performed with a two-way ANOVA with Tukey's or Bonferroni multiple comparisons post test, as appropriate for the individual experiment. Pairwise comparisons were performed with a two-tailed Student's *t*-test. A value of $P < 0.05$ was used to establish a significant difference between samples. Data in the figures are shown as mean ± SEM, unless otherwise noted.

Results

C391 is a weak, partial PAR2 agonist in RTCA and Ca^{2+} signalling assays

We modified the peptidomimetic agonist, 2-f-LIGRLO-NH_2 (McGuire *et al.*, 2004), substituting Leu_2-Ile_3-Gly_4 with an azabicycloalkane scaffold and Orn_6 with a Tyr, to create a novel peptidomimetic structure, C391 (Figure 1A, B). To evaluate the signalling effects of C391 on PAR2, we first examined its ability to activate signalling in PAR2-expressing 16HBE14o- cells using the highly sensitive xCELLigence real time cell analyser (RTCA) and Ca^{2+} imaging signalling assays (Flynn *et al.*, 2011; Boitano *et al.*, 2014). In the RTCA assay, C391 displayed a weak, partial agonist response at the highest concentration tested, with no detected responses at concentrations below 10 μM and an E_{max} that was <50% of the maximum response of an EC_{75} concentration of the potent agonist 2-at-LIGRL-NH_2 (1 μM; Figure 2A). The RTCA EC_{50} for partial activation by C391 was 17.9 μM with a 95% confidence interval (CI) of 6.2–51 μM. Similarly, in the highly sensitive Ca^{2+} imaging signalling assay, C391 induced only minimal $[Ca^{2+}]_i$ changes following addition of ≤10 μM concentrations. However, at higher concentrations, C391 induced partial activation of Ca^{2+} signalling (Figure 2B, D–G), with a reduced output compared with an EC_{75} concentration of 2-at-LIGRL-NH_2 (2 μM; Figure 2B, H–K). At E_{max} (≥30 μM), C391 could only activate 33% of cells, whereas full agonists reach 100% activation. A calculated Ca^{2+} signalling EC_{50} for partial activation by C391 was 19.6 μM (CI: 13.9–27.6 μM). C391 activity was eliminated following PAR2 desensitization with high concentrations (50 μM) of the potent agonist 2-at-LIGRL-NH_2 (Figure 2C). Such changes are consistent with specific, partial agonism of PAR2 at high concentrations of C391 (Boitano *et al.*, 2014).

C391 is a potent antagonist across signalling assays

Having determined that C391 binds PAR2 at lower concentrations without readily inducing signalling via this receptor, we sought to determine if C391 could function as a novel PAR2 antagonist. C391 was initially evaluated for PAR2 antagonist activity using the Ca^{2+} signalling assay. In these experiments, a concentration inhibition curve for C391 was constructed against an EC_{75} concentration of 2-at-LIGRL-NH_2 for Ca^{2+} activation in 16HBE14o- cells. A 2 min pretreatment of 16HBE14o- cells with C391 potently inhibited peptidomimetic-induced PAR2 Ca^{2+} signalling (Figure 3; IC_{50} = 1.30 μM, CI: 277 nM–6.07 μM), with a maximal effect observed at 3 μM. When the C391 concentration was

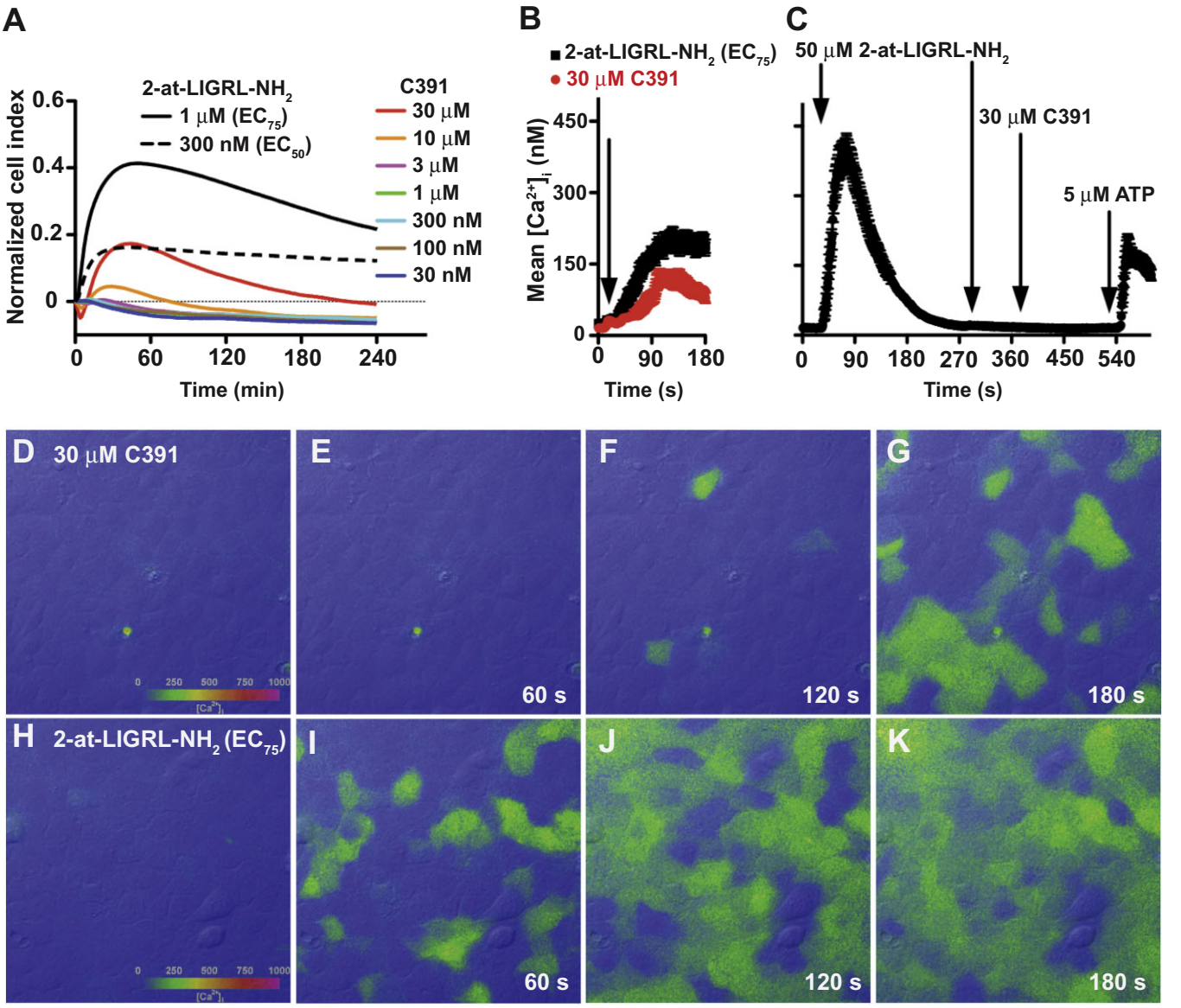

Figure 2

C391 is a weak PAR2-dependent agonist. (A) RTCA traces of PAR2 ligands on 16HBE14o- cells. C391 displays minimal activation except at high concentrations. For comparison, EC_{75} and EC_{50} responses for the potent agonist 2-at-LIGRL-NH_2 are shown. Traces are mean values from four wells from a single E-plate and are representative of at least three plates. (B) Maximum Ca^{2+} signalling responses for C391 and EC_{75} Ca^{2+} signalling response for 2-at-LIGRL-NH_2 are shown for comparison. Traces are mean values from typical experiments that include >80 cells and are plotted with their SEM. (C) PAR2 desensitization assay using 50 μM 2-at-LIGRL-NH_2 demonstrates PAR2 specificity of the C391 partial agonism response. (D–K) $[Ca^{2+}]_i$ colour maps for C391 (D–G) and 2-at-LIGRL-NH_2 (H–K) are overlaid onto a DIC image of 16HBE14o- cells for a typical ligand addition experiment. Data demonstrate partial agonism of PAR2 at high concentrations of C391.

increased to 10 μM, strong antagonism was still apparent. However, at 30 μM, C391 failed to block the effect of 2 μM 2-at-LIGRL-NH_2. This was likely to be due to the partial agonist activity observed at higher C391 concentrations, as described above.

PAR2 activates MAPK signalling through multiple pathways; this can be measured via ERK 1/2 phosphorylation (pERK). We explored whether C391 antagonized MAPK signalling using the ICW technique. As in the Ca^{2+} signalling assays, 16HBE14o- cells were pre-incubated for 2 min with a range of concentrations of C391 (300 nM–100 μM) at room temperature, followed by C391 supplemented with 2.5 μM 2-at-LIGRL-NH_2 for 5 min (Figure 4A). C391 alone did not alter pERK at any of the concentrations tested (not shown). In the presence of 2-at-LIGRL-NH_2, C391 effectively blocked pERK signalling with an IC_{50} of 14.3 μM (CI: 13.5–15.1 μM). Here, we did not observe a loss of antagonist effect at higher concentrations of C391 (30 and 100 μM), as we did in the

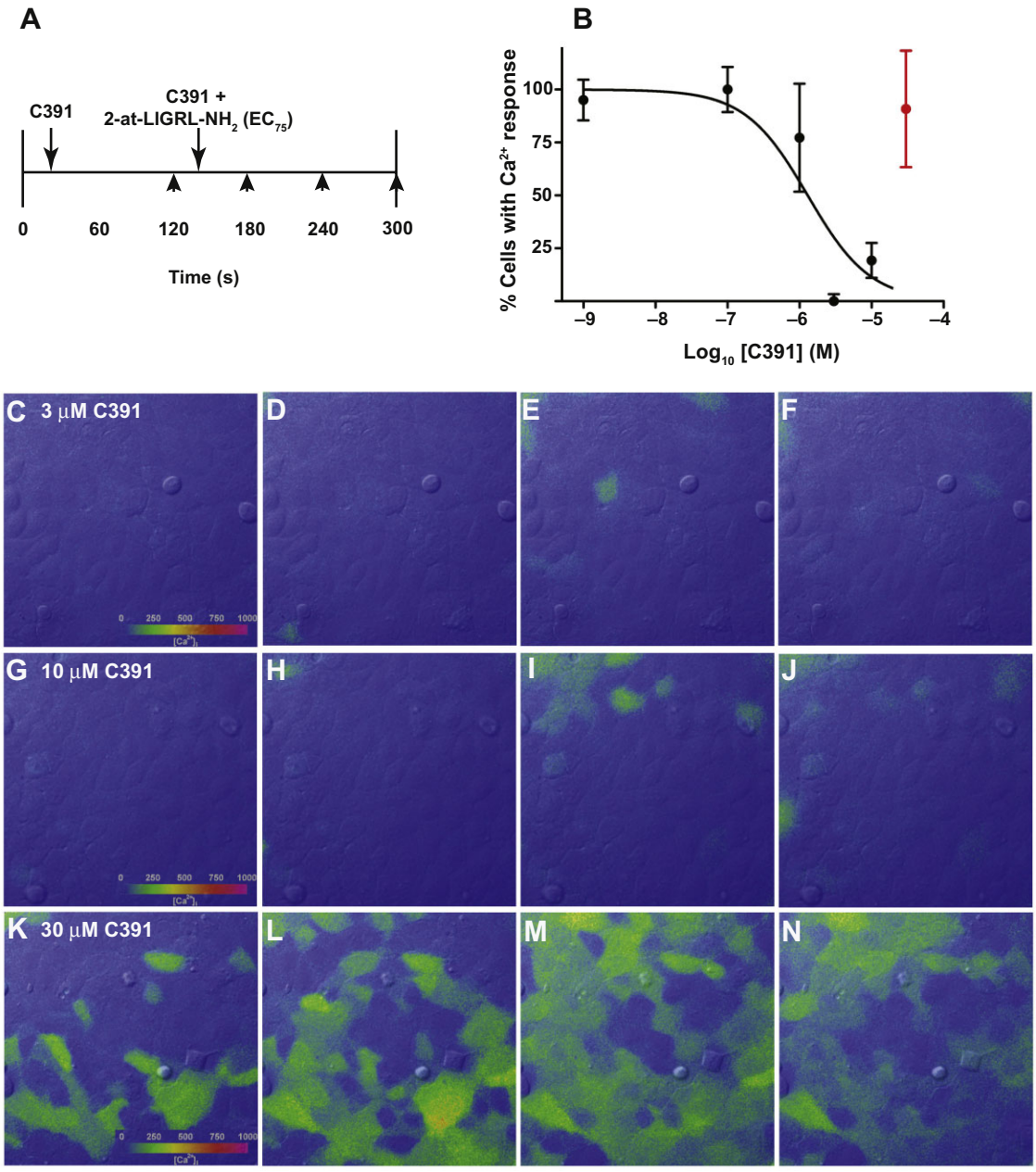

Figure 3

C391 is a potent, PAR2-dependent Ca^{2+} signalling antagonist. (A) PAR2 antagonism experimental protocol is illustrated. $[Ca^{2+}]_i$ is monitored throughout. Arrows above the axis correspond to changes in imaging medium. C391 at appropriate concentration in HBSS is introduced at 20 s. HBSS containing identical C391 concentration supplemented with an EC_{75} concentration of 2-at-LIGRL-NH_2 is introduced at 140 s. Arrowheads under the axis correspond to Ca^{2+} maps presented in C–N. (B) Percentage of cells with Ca^{2+} response between 120–300 s of the experiment are shown for each C391 concentration. Data points ($n \geq 4$) are plotted ± SEM and shown with a non-linear regression curve. Because the 30 μM concentration caused significant Ca^{2+} response, it was excluded from the curve fit. (C–N) Typical $[Ca^{2+}]_i$ over time in a group of cells treated as described in (A) with 3 μM (C–F), 10 μM (G–J), or 30 μM (H–K) C391. Colours on individual maps correspond to $[Ca^{2+}]_i$ indicated by bar in (C), (G), (K). Maps are overlaid onto DIC image of cells within the experiment to observe individual cell variability. Panels correspond to 120, 180, 240 and 300 s as indicated in (A). C391 blocks PAR2-dependent Ca^{2+} response at 3–10 μM. However, 30 μM C391 induced Ca^{2+} response and is ineffective as a PAR2-Ca^{2+} signalling antagonist.

Ca^{2+} signalling assay. To confirm the ICW results with an independent assay, we used traditional immunoblotting. As observed earlier, a full block of 2-at-LIGRL-NH_2 (2.5 μM)-induced ERK 1/2 phosphorylation was seen at higher concentrations of C391 (Figure 4B). Also as seen in the ICW, we did not observe MAPK activation by C391 in the absence of PAR2 agonist (not shown). We conclude that C391 blocked PAR2-induced MAPK signalling even at those concentrations

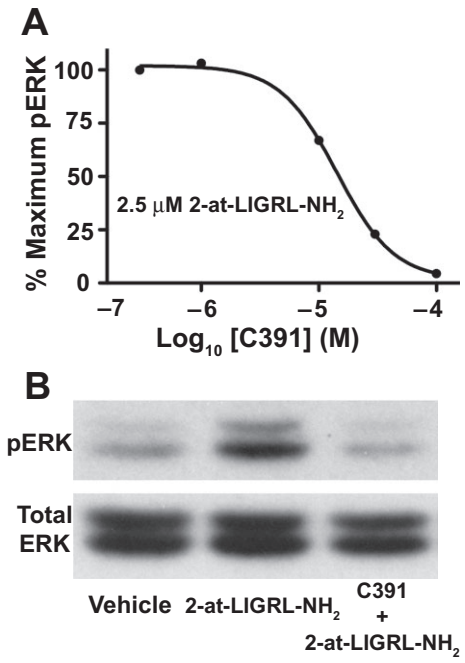

Figure 4

C391 is a potent PAR2-dependent MAPK signalling antagonist. (A) Using the results of the ICW assay, the graph shows a concentration–response curve for a 2 min pre-incubation of C391 followed by a 5 min incubation of C391 with 2.5 μM 2-at-LIGRL-NH_2. Individual points are means from n = 4 and plotted ± SEM. C391 effectively blocks 2-at-LIGRL-NH_2-induced phosphorylation of ERK 1/2. (B) Immunoblot comparison of 16HBE14o- cell lysates following a 5 min exposure to vehicle control, 2.5 μM 2-at-LIGRL-NH_2 or a 1 min pre-incubation of 100 μM C391 followed by a 5 min exposure to 2.5 μM 2-at-LIGRL-NH_2 with 100 μM C391. The data confirms C391 antagonism of 2-at-LIGRL-NH_2-induced pERK.

where partial agonist activity was observed in the Ca^{2+} signalling assay.

C391 blocks proteinase-activated PAR2

Although peptidomimetics provide potent and specific PAR2 activation, PAR2 is naturally activated *in vivo* via endogenous or exogenous trypsin-like serine proteinases (Ramachandran *et al.*, 2012). Thus, we tested if C391 could block proteinase-activated PAR2 on airway epithelial cells using trypsin. We exposed 16HBE14o- cells to sufficient trypsin to induce Ca^{2+} responses in >50% of the cells (54.4 ± 12.1%, n = 6; Figure 5A–D). Similar to that observed with the peptidomimetics, a 2 min pre-incubation with 3 μM C391 limited trypsin-induced Ca^{2+} responses to 11.6 ± 4.3% (n = 5; Figure 5E–H). This finding demonstrates that C391 attenuates PAR2 signalling induced by proteinases, likely indicating that C391 interferes with binding of the exposed tethered ligand following proteolytic cleavage of the receptor.

C391 inhibits proteinase-induced pain response in vivo

PAR2 is an important drug target for pain where the receptor is thought to regulate nociceptor excitability in response to release of endogenous proteinases associated with inflammation or other painful pathologies. Compound 48/80 induces mast cell degranulation *in vivo*, causing a PAR2-dependent thermal hyperalgesia (Vergnolle *et al.*, 2001). Hence, we tested whether compound 48/80-induced thermal hyperalgesia in mice could be blocked by C391 (Figure 6). Compound 48/80 (0.2 μg) was injected into the hindpaw of mice with or without C391 at doses ranging from 7.5 to 75 μg. Higher doses (25 and 75 μg) of C391 effectively attenuated compound 48/80-induced thermal hyperalgesia. These data confirm that C391 is a PAR2 antagonist capable of blocking proteinase-induced responses *in vivo*.

Discussion and conclusions

We have produced a novel peptidomimetic PAR2 ligand that blocks peptidomimetic and proteinase-induced PAR2-dependent G_q and downstream MAPK signalling *in vitro* as well as *in vivo* pain hypersensitivity. C391 demonstrated similar antagonist IC_{50} values in both Ca^{2+} and MAPK assays against the human receptor. Interestingly, C391 showed partial agonist activity in the Ca^{2+} assay at high concentrations but lacked this agonist activity in a MAPK assay, suggesting that it may not trigger alternate signalling pathways such as β-arrestin-dependent signalling. *In vivo*, C391 blocked mast cell degranulation-induced thermal hyperalgesia in mice, an effect that had previously been attributed to PAR2 activation using PAR2 null mice (Vergnolle *et al.*, 2001). C391 is the first PAR2 antagonist to demonstrate micromolar efficacy across signalling pathways without MAPK activation at concentrations <100 μM. Because C391 is structurally distinct from previously described PAR2 antagonists, this work elucidates a new molecular entity for PAR2 antagonist drug discovery.

A key finding from this work is that C391 has both partial agonist and antagonist activity. Moreover, this partial agonist activity appears to be pathway selective, as it was observed in Ca^{2+} signalling assays but not in MAPK assays or, in all likelihood, *in vivo*. While the traditional occupational model does not readily account for this mix of pharmacology, it may be explained by more recent views of receptor theory such as the probabilistic theory. Biased agonism has been observed at a variety of GPCRs (Kenakin, 2004; 2014; Onaran *et al.*, 2014), including PAR2 (Hollenberg *et al.*, 2014). However, examples of partial agonist/antagonist mixed activity observed herein for C391 and other PAR2 antagonists (Goh *et al.*, 2009; Hollenberg *et al.*, 2014; Suen *et al.*, 2014) are less well defined (Kenakin, 2014). One possibility is that C391 is not a biased ligand; rather it is a weak partial agonist for Ca^{2+} signalling and MAPK activity with our MAPK signalling assessment lacking sufficient sensitivity to detect compound activity. This is a distinct possibility based upon the real-time resolution of digital Ca^{2+} imaging, and the well-accepted sensitivity of this assay. In this case, C391 would have a binding affinity for PAR2 far to the left of its EC_{50} for G protein signalling activation [defined as a small intrinsic activity (tau) value in the original operational model (Black and Leff, 1983)]. Therefore, the compound would act as a neutral antagonist at most concentrations due to its weak intrinsic

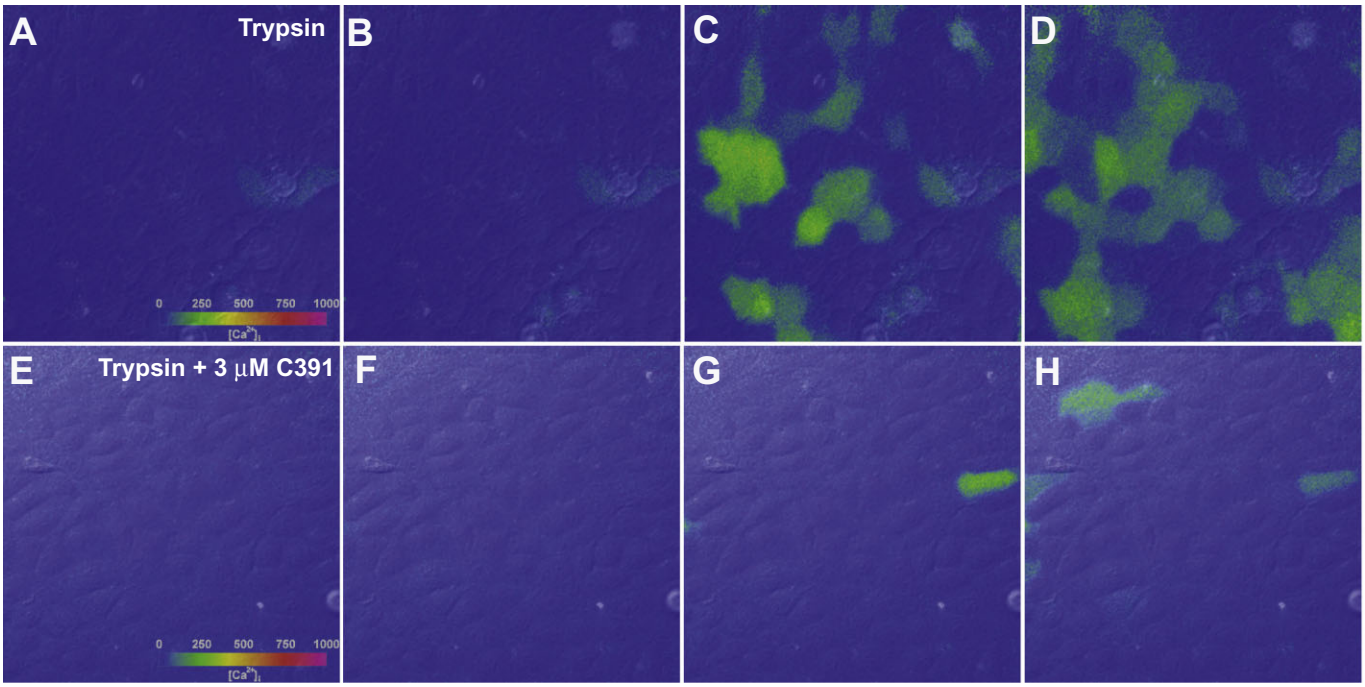

Figure 5

C391 antagonizes trypsin proteinase signalling at PAR2. (A–D) Changes in $[Ca^{2+}]_i$ are shown as colour maps over time in response to trypsin. Individual panels are from 20 s before trypsin addition and at 60 s intervals. (E–H) The same experiment as (A) but with a 2 min pre-incubation with 3 μM C391 and continued 3 μM C391 treatment during trypsin exposure. C391 blocks proteinase-induced Ca^{2+} changes.

activity. Our *in vivo* findings are consistent with this being the dominant action of the compound even at very high local concentrations.

While several antagonists of PAR2 have been proposed in the literature or in patent applications (Yau *et al.*, 2013), few have been investigated across PAR2 signalling pathways and/or for *in vivo* efficacy. Those antagonists that have been investigated across multiple signalling pathways include K-14585: N-[1-(2,6-dichlorophenyl)methyl]-3-(1-pyrrolidinylmethyl)-1H-indol-5-yl]aminocarbonyl}-glycinyl-L-lysinyl-L-phenylalanyl-N-benzhydrylamide (Goh *et al.*, 2009; Kanke *et al.*, 2009) and GB88: 5-isoxazoyl-Cha-Ile-spriroindene-1,4,-piperidine (Suen *et al.*, 2010; 2014; Hollenberg *et al.*, 2014). These compounds provide baseline comparisons for the newly developed C391. K-14585 can block peptide and/or peptidomimetic-induced G_q-associated Ca^{2+} signalling following a 15 min pre-incubation in PAR2-expressing NCT2544 cells (Kanke *et al.*, 2009; Suen *et al.*, 2010). Notably, at 5 and 30 μM, K-14585 reduced SLIGKV-OH-induced inositol phosphate production by 65–70% in these cells. However, K-14585 was much less effective against trypsin-activated PAR2, reducing a 30 nM trypsin-induced inositol phosphate signal by a maximum of 20%. In contrast, K-14585 displayed agonistic effects on p38 MAP kinase (and to a lesser effect, ERK 1/2) in the absence of PAR2-stimulating peptides. Despite an incomplete block of Ca^{2+} signalling and an agonism of MAPK at micromolar concentrations, K-14585 blocked *in situ* and *in vivo* physiological effects attributed to PAR2 (Kanke *et al.*, 2009). An improved peptidomimetic PAR2 antagonist, GB88, effectively blocked both peptide and proteinase-induced Ca^{2+} signalling in a variety of cell types following a 15 min pre-incubation. This compound also inhibited PAR2-associated rat paw oedema (Suen *et al.*, 2012) and was effective after oral administration in a chronic arthritis model in rats (Lohman *et al.*, 2012). Subsequent studies of this Ca^{2+}-signalling antagonist demonstrated that it too acted as an agonist of ERK 1/2 signalling in addition to other PAR2-associated pathways (Suen *et al.*, 2014). When tested in our more sensitive digital imaging microscopy analysis of Ca^{2+} signalling on 16HBE14o- cells under 2–3 min pre-incubation times for a direct comparison with C391 antagonism reported herein, GB88 did not block Ca^{2+} signalling at concentrations up to 60 μM (data not shown). Under conditions of a 15 min pre-incubation, as reported to be necessary for GB88 antagonism (Suen *et al.*, 2012), GB88 did block Ca^{2+} signalling in our assay (Supporting Information Fig. S1). However, inhibiting concentrations of GB88 (30 μM, 10 μM and, to a lesser extent, 3 μM) included pre-activation of Ca^{2+} signalling in most of the 16HBE14o- cells between 2 and 6 min following initial application of GB88 (Supporting Information Fig. S1). These data suggest, at least at human PAR2, that GB88 acts as a partial or full Ca^{2+} agonist. In contrast, we found that a short pre-incubation (2 min) of 3 μM C391 was sufficient for full block of Ca^{2+} signalling induced by peptide or proteinase agonists (Figures 3 and 5). In summary, C391 differs from both K-14585 and GB88 in that it requires minimal pre-incubation for antagonism of peptide/peptidomimetic activation of PAR2-dependent Ca^{2+} signalling and it acts as an antagonist for MAPK signalling pathways, without any signs of activation, up to the 100 μM

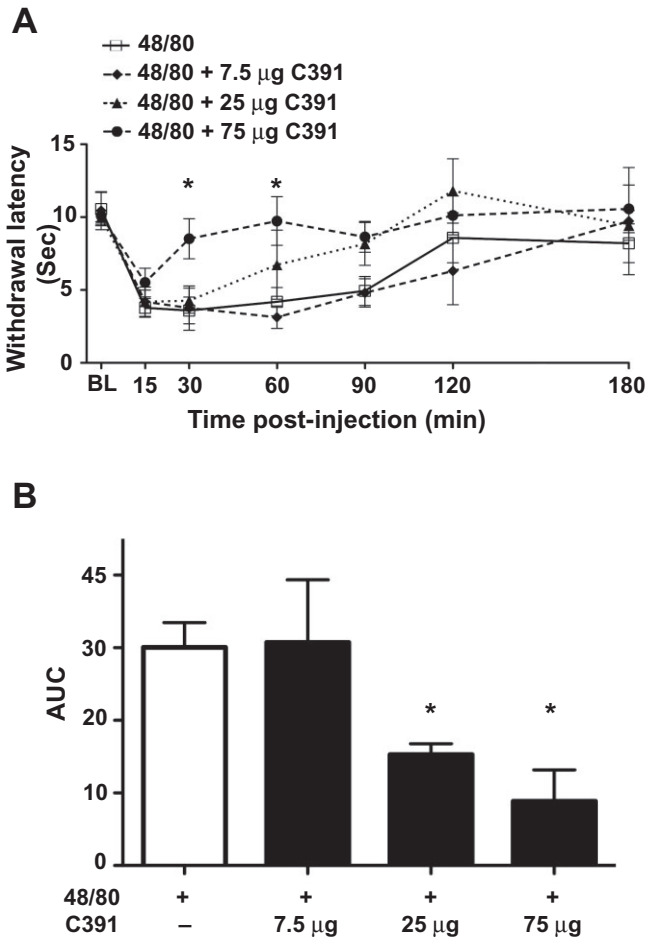

Figure 6

C391 antagonizes proteinase-dependent thermal hyperalgesia *in vivo*. Mice received intraplantar injections of Compound 48/80 (0.2 μg) with or without the indicated doses of C391 and thermal sensitivity was measured over the ensuing 3 h time period. Thermal latencies are shown in (A) and quantified AUC data in (B). *$P < 0.05$, two-way ANOVA with Bonferroni *post hoc* test. $n = 3–8$ per group.

concentrations tested. It should be noted that PAR2 activation has been associated with G_i and $G_{12/13}$ to induce cAMP and RhoA signalling, respectively, and that GB88 has been shown to act as a PAR2 agonist on these pathways (Suen *et al.*, 2014). Further studies are required to evaluate the effects, if any, of C391 on these PAR2-dependent responses.

C391 blocked Ca^{2+} and MAPK signalling induced by peptide/peptidomimetics and inhibited PAR2 activation induced by proteolytic cleavage of the N-terminus of the receptor. This is crucial because the mode of action of PAR2 activation *in vivo* is exposure to either exogenous or endogenous proteinases. A clinical situation where exposure to exogenous proteinases contributes to pathology is in allergy-associated asthma. Several asthma-associated allergens, including those from house dust mite, cockroach and *Alternaria alternata*, contain trypsin-like serine proteinases that can cleave and activate PAR2 signalling *in vitro* and in animal models (Schmidlin *et al.*, 2002; Takizawa *et al.*, 2005; Day *et al.*, 2010; Page *et al.*, 2010; Boitano *et al.*, 2011; Nichols *et al.*, 2012; Snelgrove *et al.*, 2014). We have demonstrated here that C391 blocked trypsin-induced PAR2 signalling. Another clinical example of exposure to endogenous proteinases playing a key role in pathology is during inflammation. Proteinases secreted by immune cells during the inflammation process strongly sensitize peripheral nociceptors, causing inflammatory pain. PAR2 is central to this process, as demonstrated in $PAR2^{-/-}$ mice (Vergnolle *et al.*, 2001). Our findings with the model of thermal hyperalgesia following mast cell degranulation showed that acute antagonism of PAR2 nearly abolished this enhancement in thermal pain sensitivity. These results serve as a proof of concept for further development of PAR2 antagonists as treatments for inflammatory and possibly other types of pain, including visceral and cancer pain.

In conclusion, we have described here a novel, potent and specific antagonist of PAR2, derived by changes to the structure of existing PAR2 agonists. This compound, C391, exhibited PAR2 antagonist properties in the low micromolar range, with some indication of weak partial agonist activity emerging at mid-micromolar concentrations. Despite this weak partial agonist activity, the compound displayed antagonist activity in different signalling assays and *in vivo*. We conclude that C391 acts as a neutral, orthosteric antagonist of PAR2 at most concentrations, making this compound a new prototype for the further development of PAR2 antagonists.

Acknowledgements

We would like to thank Daniel X. Sherwood for his programme that allowed for quick quantification of Ca^{2+} data. This work was primarily funded by a multi-PI grant (NS 073664 to S. B., J. V. and T. J. P.) from the National Institutes of Health. Additional support for this work was from the following grants: National Institute of Health training grants (T32 HL 007249 for A. N. F.; T32 ES 007091 for C. L. S.; and R25 GM 062584 for C. M. R.), National Institutes of Health R01NS 065926 (T. J. P.) and R01AI083403 (S. B.; Michael O. Daines, PI), State of Arizona Technology and Research Initiative Fund awarded through Bio5 (J. V.). Funds to purchase the RTCA were provided through the National Institutes of Health Grant ES 04940 (NIEHS Superfund) and by the State of Arizona Technology and Research Initiative Fund awarded through the Water Sustainability Program.

Author contributions

S. B., J. H., A. N. F., M. N. A., D. V. T., Z. Z., C. L. S., C. M. R., K. A. D. and J. V. performed the research. S. B., K. A. D., J. V. and T. J. P. designed the research study. S. B., K. A. D., J. V. and T. J. P. contributed essential reagents and tools. S. B., J. H., C. L. S., C. M. R., K. A. D. and T. J. P. analysed the data. S. B., J. H., J. V., K. A. D., T. J. P. wrote the paper.

Conflict of interest

None to declare.

References

Adams MN, Ramachandran R, Yau MK, Suen JY, Fairlie DP, Hollenberg MD *et al*. (2011). Structure, function and pathophysiology of protease activated receptors. Pharmacol Ther 130: 248–282.

Alexander SP, Benson HE, Faccenda E, Pawson AJ, Sharman JL, Spedding M *et al*. (2013a). The concise guide to PHARMACOLOGY 2013/14: G protein-coupled receptors. Br J Pharmacol 170: 1459–1581.

Alexander SPH, Benson HE, Faccenda E, Pawson AJ, Sharman JL, Spedding M *et al*. (2013b). The Concise Guide to PHARMACOLOGY 2013/14: Enzymes. Br J Pharmacol 170: 1797–1867.

Atherton E, Logan C, Sheppard R (1981). Peptide synthesis. Part 2. Procedures for solid-phase synthesis using Na-fluorenylmethoxycarbonylamino-acids on polyamide supports. Synthesis of substance P and of acyl carrier protein 65–74 decapeptide. J Chem Soc [Perkin] 1: 538–546.

Atienza JM, Zhu J, Wang X, Xu X, Abassi Y (2005). Dynamic monitoring of cell adhesion and spreading on microelectronic sensor arrays. J Biomol Screen 10: 795–805.

Bao Y, Hou W, Hua B (2014). Protease-activated receptor 2 signalling pathways: a role in pain processing. Expert Opin Ther Targets 18: 15–27.

Barry GD, Suen JY, Le GT, Cotterell A, Reid RC, Fairlie DP (2010). Novel agonists and antagonists for human protease activated receptor 2. J Med Chem 53: 7428–7440.

Black JW, Leff P (1983). Operational models of pharmacological agonism. Proc R Soc Lond B Biol Sci 220: 141–162.

Boitano S, Flynn AN, Sherwood CL, Schulz SM, Hoffman J, Gruzinova I *et al*. (2011). *Alternaria alternata* serine proteases induce lung inflammation and airway epithelial cell activation via PAR2. Am J Physiol Lung Cell Mol Physiol 300: L605–L614.

Boitano S, Hoffman J, Tillu DV, Asiedu MN, Zhang Z, Sherwood CL *et al*. (2014). Development and evaluation of small peptidomimetic ligands to protease-activated receptor-2 (PAR_2) through the use of lipid tethering. PLoS ONE 9: e99140.

Dai Y, Moriyama T, Higashi T, Togashi K, Kobayashi K, Yamanaka H *et al*. (2004). Proteinase-activated receptor 2-mediated potentiation of transient receptor potential vanilloid subfamily 1 activity reveals a mechanism for proteinase-induced inflammatory pain. J Neurosci 24: 4293–4299.

Day SB, Zhou P, Ledford JR, Page K (2010). German cockroach frass proteases modulate the innate immune response via activation of protease-activated receptor-2. J Innate Immun 2: 495–504.

Flynn AN, Tillu DV, Asiedu MN, Hoffman J, Vagner J, Price TJ *et al*. (2011). The protease-activated receptor-2-specific agonists 2-aminothiazol-4-yl-LIGRL-NH_2 and 6-aminonicotinyl-LIGRL-NH_2 stimulate multiple signaling pathways to induce physiological responses *in vitro* and *in vivo*. J Biol Chem 286: 19076–19088.

Flynn AN, Hoffman J, Tillu DV, Sherwood CL, Zhang Z, Patek R *et al*. (2013). Development of highly potent protease-activated receptor 2 agonists via synthetic lipid tethering. FASEB J 27: 1498–1510.

Goh FG, Ng PY, Nilsson M, Kanke T, Plevin R (2009). Dual effect of the novel peptide antagonist K-14585 on proteinase-activated receptor-2-mediated signalling. Br J Pharmacol 158: 1695–1704.

Gruenert DC, Finkbeiner WE, Widdicombe JH (1995). Culture and transformation of human airway epithelial cells. Am J Physiol 268 (3 Pt 1): L347–L360.

Grynkiewicz G, Poenie M, Tsien RY (1985). A new generation of Ca^{2+} indicators with greatly improved fluorescence properties. J Biol Chem 260: 3440–3450.

Hargreaves K, Dubner R, Brown F, Flores C, Joris J (1988). A new and sensitive method for measuring thermal nociception in cutaneous hyperalgesia. Pain 32: 77–88.

Hoffman J, Flynn A, Tillu D, Zhang Z, Patek R, Price T *et al*. (2012). Lanthanide labeling of a potent protease activated receptor-2 agonist for time-resolved fluorescence analysis. Bioconjug Chem 23: 2098–2104.

Hollenberg MD, Mihara K, Polley D, Suen JY, Han A, Fairlie DP *et al*. (2014). Biased signalling and proteinase-activated receptors (PARs): targeting inflammatory disease. Br J Pharmacol 171: 1180–1194.

Jacquet A (2011). Interactions of airway epithelium with protease allergens in the allergic response. Clin Exp Allergy 41: 305–311.

Kanke T, Kabeya M, Kubo S, Kondo S, Yasuoka K, Tagashira J *et al*. (2009). Novel antagonists for proteinase-activated receptor 2: inhibition of cellular and vascular responses *in vitro* and *in vivo*. Br J Pharmacol 158: 361–371.

Kenakin T (2004). Principles: receptor theory in pharmacology. Trends Pharmacol Sci 25: 186–192.

Kenakin T (2014). What is pharmacological 'affinity'? Relevance to biased agonism and antagonism. Trends Pharmacol Sci 35: 434–441.

Kilkenny C, Browne WJ, Cuthill IC, Emerson M, Altman DG (2010). Improving bioscience research reporting: the ARRIVE guidelines for reporting animal research. PLoS Biol 8: e1000412.

Lohman RJ, Cotterell AJ, Barry GD, Liu L, Suen JY, Vesey DA *et al*. (2012). An antagonist of human protease activated receptor-2 attenuates PAR2 signaling, macrophage activation, mast cell degranulation, and collagen-induced arthritis in rats. FASEB J 26: 2877–2887.

McGrath J, Drummond G, McLachlan E, Kilkenny C, Wainwright C (2010). Guidelines for reporting experiments involving animals: the ARRIVE guidelines. Br J Pharmacol 160: 1573–1576.

McGuire JJ, Saifeddine M, Triggle CR, Sun K, Hollenberg MD (2004). 2-furoyl-LIGRLO-amide: a potent and selective proteinase-activated receptor 2 agonist. J Pharmacol Exp Ther 309: 1124–1131.

Nichols HL, Saffeddine M, Theriot BS, Hegde A, Polley D, El-Mays T *et al*. (2012). beta-Arrestin-2 mediates the proinflammatory effects of proteinase-activated receptor-2 in the airway. Proc Natl Acad Sci U S A 109: 16660–16665.

Onaran HO, Rajagopal S, Costa T (2014). What is biased efficacy? Defining the relationship between intrinsic efficacy and free energy coupling. Trends Pharmacol Sci 35: 639–647.

Page K, Ledford JR, Zhou P, Dienger K, Wills-Karp M (2010). Mucosal sensitization to German cockroach involves protease-activated receptor-2. Respir Res 11: 62.

Pawson AJ, Sharman JL, Benson HE, Faccenda E, Alexander SP, Buneman OP *et al*.; NC-IUPHAR (2014). The IUPHAR/BPS Guide to PHARMACOLOGY: an expert-driven knowledge base of drug targets and their ligands. Nucl Acids Res 42 (Database Issue): D1098–D1106.

Ramachandran R, Noorbakhsh F, Defea K, Hollenberg MD (2012). Targeting proteinase-activated receptors: therapeutic potential and challenges. Nat Rev Drug Discov 11: 69–86.

Reed CE, Kita H (2004). The role of protease activation of inflammation in allergic respiratory diseases. J Allergy Clin Immunol 114: 997–1008, quiz 1009.

Schmidlin F, Amadesi S, Dabbagh K, Lewis DE, Knott P, Bunnett NW *et al.* (2002). Protease-activated receptor 2 mediates eosinophil infiltration and hyperreactivity in allergic inflammation of the airway. J Immunol 169: 5315–5321.

Snelgrove RJ, Gregory LG, Peiro T, Akthar S, Campbell GA, Walker SA *et al.* (2014). Alternaria-derived serine protease activity drives IL-33 mediated asthma exacerbations. J Allergy Clin Immunol 134: 583–592.

Suen JY, Gardiner B, Grimmond S, Fairlie DP (2010). Profiling gene expression induced by protease-activated receptor 2 (PAR2) activation in human kidney cells. PLoS ONE 5: e13809.

Suen JY, Barry GD, Lohman RJ, Halili MA, Cotterell AJ, Le GT *et al.* (2012). Modulating human proteinase activated receptor 2 with a novel antagonist (GB88) and agonist (GB110). Br J Pharmacol 165: 1413–1423.

Suen JY, Cotterell A, Lohman RJ, Lim J, Han A, Yau MK *et al.* (2014). Pathway-selective antagonism of proteinase activated receptor 2. Br J Pharmacol 171: 4112–4124.

Takizawa T, Tamiya M, Hara T, Matsumoto J, Saito N, Kanke T *et al.* (2005). Abrogation of bronchial eosinophilic inflammation and attenuated eotaxin content in protease-activated receptor 2-deficient mice. J Pharmacol Sci 98: 99–102.

Tillu DV, Hassler SN, Burgos-Vega CC, Quinn TL, Sorge RE, Dussor G *et al.* (2015). Protease-activated receptor 2 activation is sufficient to induce the transition to a chronic pain state. Pain 156: 859–867.

Vergnolle N (2009). Protease-activated receptors as drug targets in inflammation and pain. Pharmacol Ther 123: 292–309.

Vergnolle N, Bunnett NW, Sharkey KA, Brussee V, Compton SJ, Grady EF *et al.* (2001). Proteinase-activated receptor-2 and hyperalgesia: a novel pain pathway. Nat Med 7: 821–826.

Yau MK, Liu L, Fairlie DP (2013). Toward drugs for protease-activated receptor 2 (PAR2). J Med Chem 56: 7477–7497.

Supporting information

Additional Supporting Information may be found in the online version of this article at the publisher's web-site:

http://dx.doi.org/10.1111/bph.13238

Figure S1 Digital Ca^{2+} imaging microscopy analysis of GB88 on 16HBE14o- cells. (A) The experimental procedure used for GB88 Ca^{2+} imaging is shown. GB88 was added at 1 min and allowed to interact with 16HBE14o- cells for an additional 15 min. At time 16:20, GB88 supplemented with an EC_{75} concentration of 2-at-LIGRL-NH_2 was added. At 19 min, ATP was added to demonstrate PAR2-independent Ca^{2+} signalling remained intact. (B) Typical experiment showing mean $[Ca^{2+}]_i$ is plotted over time in response to 30 μM GB88. 30 μM GB88 alone induced 72.1 ± 12.1% Ca^{2+} response prior to 2-at-LIGRL-NH_2 addition, while reducing peptidomimetic activation to 29.8 ± 28.3% (i.e. time 16–19 min; n = 3). (C) Typical experiment showing mean $[Ca^{2+}]_i$ is plotted over time in response to 10 μM GB88. 10 μM GB88 alone evoked a 92.4 ± 2.3% Ca^{2+} response prior to 2-at-LIGRL-NH_2 addition, while reducing peptidomimetic activation to 44.4 ± 22.2% (n = 3). (D) A typical experiment showing mean $[Ca^{2+}]_i$ is plotted over time in response to 3 μM GB88. 3 μM GB88 alone caused a 42.1 ± 12.1% Ca^{2+} response prior to 2-at-LIGRL-NH_2 addition, while reducing peptidomimetic activation to 12.6 ± 10.0% (n = 4). When 2-at-LIGRL-NH_2 was added in the absence of GB88 and analysed over a 3 min experiment, it resulted in a Ca^{2+} response of 72.9 ± 11.4% (n = 5).